

Type-II superconductivity in W_5Si_3 -type Nb_5Sn_2Al

Jifeng Wu^{1,2}, Bin Liu^{1,2}, Yanwei Cui², Hangdong Wang⁴,
Zhicheng Wang³, Zhi Ren^{2†}, Guanghan Cao³

¹Department of Physics, Fudan University, Shanghai 200433, P. R. China

²School of Science, Westlake Institute for Advanced Study, Westlake University, 18 Shilongshan Road, Hangzhou 310064, P. R. China

³Department of Physics, Zhejiang University, Hangzhou 310027, P. R. China

⁴Department of Physics, Hangzhou Normal University, Hangzhou 310036, P. R. China

Abstract. We report the discovery of superconductivity in the ternary aluminide Nb_5Sn_2Al , which crystallizes in the W_5Si_3 -type structure with one-dimensional Nb chains along the c -axis. It is found that the compound has a multiband nature and becomes a weakly coupled, type-II superconductor below 2.0 K. The bulk nature of superconductivity is confirmed by the specific heat jump, whose temperature dependence shows apparent deviation from a single isotropic gap behavior. The lower and upper critical fields are estimated to be 2.0 mT and 0.3 T, respectively. From these values, we derive the penetration depth, coherence length and Ginzburg-Landau parameter to be 516 nm, 32.8 nm and 15.6, respectively. By contrast, the isostructural compound Ti_5Sn_2Al does not superconduct above 0.5 K. A comparison of these results with other W_5Si_3 -type superconductors suggests that T_c of these compounds correlates with the average number of valence electrons per atom.

PACS numbers: 74.10.-v, 74.25.-q, 74.70.Dd

† Electronic address: zhi.ren@wias.org.cn

1. Introduction

Some structural types have been shown to favor the occurrence of superconductivity (SC) in intermetallic compounds [1]. A well-known example is the cubic $A15$ materials with the general formula A_3B , in which nearly fifty superconductors were found and the highest T_c reaches above 20 K [2]. Recently, the A_5B_3 compounds and their derivatives emerge as another fertile ground for SC [3, 4, 5, 6, 7, 8, 9, 10, 11, 12, 13, 14, 15, 16]. These materials mainly crystallize in three different structural types, namely, tetragonal Cr_5B_3 -type [17], W_5Si_3 -type [18], and hexagonal Mn_5Si_3 -type [19]. In particular, the W_5Si_3 and $A15$ types are similar in that they both consist of one dimensional chains of the A atoms, which could give rise to a large density of states at the Fermi level [$N(E_F)$] [20]. So far, except for W_5Si_3 itself [9], superconductors of this structural type include Nb_5X_3 ($X=Si, Ge$ and Ga) [3, 4, 5], Nb_5Sn_2Ga [7], Ta_5Ga_2Sn [8], $Hf_5Sb_{2.5}Ru_{0.5}$ [13], and $Zr_5Sb_{2.4}Ru_{0.6}$ [14]. The exploration and study of new member will help to identify the factors that govern T_c in these materials.

Ternary aluminides Nb_5Sn_2Al and Ti_5Sn_2Al were first synthesized in 1990s and found to adopt the W_5Si_3 -type structure [21]. However, to our knowledge, their physical properties have not been investigated to date. In this paper, we present measurements of resistivity, Hall coefficient, magnetic susceptibility and specific heat on high-quality polycrystalline samples of Nb_5Sn_2Al and Ti_5Sn_2Al . We show that Nb_5Sn_2Al is a type-II superconductor with T_c of 2.0 K, and the behavior of its specific heat jump is inconsistent with Bardeen-Cooper-Schreiffer (BCS) prediction for a single isotropic gap. Nevertheless, the isostructural Ti_5Sn_2Al with remains normal down to 0.5 K, albeit with a larger Sommerfeld coefficient. We compare these results with other W_5Si_3 -type superconductors and discuss the dependence of their T_c on the valence electron count.

2. Experimental

Polycrystalline M_5Sn_2Al ($M= Nb, Ti$) samples were synthesized by using a solid state reaction method, similar to the previous report [21]. High purity powders of M (99.99%), Sn (99.99%) and Al (99.999%) with the stoichiometric ratio of 5:2:1 were homogenized and pressed into pellets in an argon-filled glove-box. The pellets were then loaded in an alumina crucible, which was sealed in a tantalum (Ta) tube. The Ta tube was protected in a argon-filled sealed quartz tube, which was heated to 900-1000 °C in a muffle furnace. After maintaining for 10 days, the quartz tube was quenched into cold water. The reaction was repeated for several times with intermediate grinding to ensure sample homogeneity.

The purity of the resulting M_5Sn_2Al samples was checked by powder X-ray diffraction (XRD) using a PANalytical x-ray diffractometer with a monochromatic $Cu-K_{\alpha 1}$ radiation at room temperature. The chemical compositions of these samples were measured with an energy-dispersive X-ray (EDX) spectrometer (Model Octane Plus). The spectra were collected on different locations of each sample, and the Al content was

not included in the analysis due to contribution from Al sample holders. For consistency reason, all the physical property measurements were performed on samples derived from the same pellet. A part of the pellet was cut into regular-shaped samples for transport and specific heat measurements, and the remaining part was crushed into powders. The electrical resistivity was measured using a standard four-probe method. Resistivity, Hall coefficient and specific heat measurements down to 1.8 K were performed on a Quantum Design PPMS-9 Dynacool. Measurements of resistivity and specific heat down to 0.5 K were carried out on a Quantum Design PPMS-9 Evercool II. The two sets of specific-heat data agree well within 5% in the overlapped temperature range. The dc magnetization was measured on crushed powders with a commercial SQUID magnetometer (Quantum Design MPMS3).

3. Results

3.1. Crystal Structure and chemical composition

The structure of M_5Sn_2Al is sketched in Fig. 1(a) and (b). All the atoms are distributed orderly in the lattice, and there are two distinct crystallographic sites for the M atoms, namely $M(1)$ at $16k$ site and $M(2)$ at $4b$ site. Notably, these atoms form linear and zigzag chains along the c -axis, respectively. For Nb_5Sn_2Al , this one dimensional arrangement of Nb atoms is reminiscent of that observed in Nb_3Sn . Figure 1(c) shows the XRD patterns of the Nb_5Sn_2Al and Ti_5Sn_2Al samples at room temperature, together with structural refinement profiles using the GSAS program. The observed and calculated diffraction patterns show a good agreement for both cases, demonstrating that they adopt the tetragonal W_5Si_3 -type structure. As can be seen in Table 1, the refined lattice parameters are $a = 10.638 \text{ \AA}$, $c = 5.225 \text{ \AA}$ for Nb_5Sn_2Al and $a = 10.558 \text{ \AA}$, $c = 5.262 \text{ \AA}$ for Ti_5Sn_2Al , which are in good agreement with the previous report [21]. It is also noted that, for Ti_5Sn_2Al , there exists additional diffraction peaks due to unknown impurities, whose maximum intensity is around one tenth that of the main phase. This suggests that the impurity phases occupy $\sim 10\%$ of the sample volume. On the other hand, EDX measurements yield the Nb:Sn molar ratio of 5:2.06(6) and Ti:Sn ratio of 5:2.09(3) for the Nb_5Sn_2Al and Ti_5Sn_2Al samples, respectively. These results indicate that both compounds are stoichiometric within the experimental error. In addition, a Ti:Sn ratio in the range of 5:2.55–2.80 is observed in a small part of the Ti_5Sn_2Al sample, which is presumably ascribed to the impurities detected in XRD.

3.2. Resistivity and Hall coefficient

Figure 2(a) shows the temperature dependence of resistivity for Nb_5Sn_2Al and Ti_5Sn_2Al . For both samples, the resistivity shows a weak metallic behavior with a concave curvature, similar to that observed in other A_5B_3 compounds [10, 11, 12, 15]. Actually, the data of Nb_5Sn_2Al is an almost rigid upward shift of that of Ti_5Sn_2Al , pointing to essentially the same temperature-dependent electron scattering mechanism for the two

samples. However, their low temperature behavior is quite different. As can be seen in the inset of Fig. 2(a), when cooling below 2.5 K, the resistivity of Nb_5Sn_2Al drops rapidly to zero, evidencing a superconducting transition. By contrast, for Ti_5Sn_2Al , the decrease in resistivity tends to saturate and no SC is observed down to 0.5 K.

Figure 2(b) shows the temperature dependence of $1/(eR_H)$ for the two samples, where e is the electron charge and R_H is the low-field Hall coefficient. The R_H of Nb_5Sn_2Al is negative at room temperature and becomes positive below 200 K. A similar sign reversal in R_H is observed for Ti_5Sn_2Al , but its R_H changes back to negative again at ~ 100 K. These results provide clear evidence that these materials are multiband systems with both electrons and holes. Nevertheless, at temperatures below 50 K, R_H is nearly temperature independent and the Hall resistivity is linear with magnetic field [see the inset of Fig. 2(b)] for both samples. Hence it appears that, in this temperature range, their electrical transport is dominated by a single type of carriers. Assuming a one-band model, the hole and electron densities are estimated to be $1.3 \times 10^{22} \text{ cm}^{-3}$ and $1.5 \times 10^{22} \text{ cm}^{-3}$ for Nb_5Sn_2Al and Ti_5Sn_2Al , respectively.

3.3. Magnetic susceptibility

The occurrence of SC in Nb_5Sn_2Al is corroborated by the magnetic susceptibility results of powder samples shown in Fig. 3. Here the demagnetization effect is taken into consideration assuming that the powders consist of cubic-shaped grains with the demagnetization factor $N_d = 0.3$. A strong diamagnetic signal is observed in both field-cooling (FC) and zero-field cooling (ZFC) data. In addition, a divergence is seen between the ZFC and FC curves, which is characteristic of a type-II superconducting behavior. The linear extrapolation of the initial ZFC diamagnetic transition intersects with the baseline at 2.0 K (see the inset of Fig. 3), which coincides with the onset of zero resistivity. In light of this coincidence, we determine T_c as 2.0 K for Nb_5Sn_2Al . At 0.4 K, the ZFC and FC data correspond to shielding and Meissner fractions of 85% and 22%, respectively, and hence clearly indicate bulk SC.

3.4. Specific heat

Figure 4(a) shows the low temperature specific heat data for Nb_5Sn_2Al and Ti_5Sn_2Al . A strong anomaly is observed in Nb_5Sn_2Al near its T_c , which further confirms the bulk nature of SC. On the other hand, its normal state data can be well described by the Debye model $C_p/T = \gamma + \beta T^2$, where γ and β are the Sommerfeld and phonon specific heat coefficients, respectively. The fit yields $\gamma = 19.0 \text{ mJ mol}^{-1} \text{ K}^{-2}$ and $\beta = 0.396 \text{ mJ mol}^{-1} \text{ K}^{-4}$. The Debye temperature Θ_D is then calculated as $\Theta_D = (12\pi^4 NR/5\beta)^{\frac{1}{3}} = 340 \text{ K}$, where $N = 8$ and R is the molar gas constant $8.314 \text{ J mol}^{-1} \text{ K}^{-1}$. Applying the same analysis to the data of Ti_5Sn_2Al gives $\gamma = 31.5 \text{ mJ mol}^{-1} \text{ K}^{-2}$, $\beta = 0.2709 \text{ mJ mol}^{-1} \text{ K}^{-4}$, and $\Theta_D = 386 \text{ K}$. Compared with Nb_5Sn_2Al , the larger Θ_D of Ti_5Sn_2Al is as expected, but its larger γ value is somewhat surprising.

Figure 4(b) shows the normalized electronic specific heat of Nb_5Sn_2Al at zero field after subtraction of the phonon contribution, plotted a function of reduced temperature T/T_c . One can see that the normalized specific heat jump $\Delta C_{el}/\gamma T_c \sim 0.86$ is considerably smaller than the BCS value of 1.43 [22]. Furthermore, the temperature dependence of the specific heat jump shows a significant deviation from the BCS theory, especially in the low temperature region. Note that an extrapolation of $C_{el}/\gamma T$ to 0 K yields a negative value. This, together with the absence of additional XRD peaks from impurities [see Fig. 1(c)], suggests that the sample has a superconducting volume fraction close to 100%. It therefore appears that the small specific heat jump is of intrinsic origin, which points to the presence of multiple gaps as in MgB_2 [23] and $Lu_2Fe_3Si_5$ [24], or even gap nodes. Nevertheless, the $C_{el}/\gamma T$ data at 0.5 K is still as large as 50% of its normal-state value, and hence to distinguish these scenarios, C_p/T measurements down to mK range would be needed.

Assuming that SC in Nb_5Sn_2Al is mediated by electron-phonon coupling, the corresponding constant, λ_{ph} , can be estimated by using the inverted McMillan formula [25],

$$\lambda_{ph} = \frac{1.04 + \mu^* \ln(\Theta_D/1.45 T_c)}{(1 - 0.62\mu^*) \ln(\Theta_D/1.45 T_c) - 1.04}, \quad (1)$$

where μ^* is the Coulomb repulsion pseudopotential. Taking an empirical μ^* value of 0.13, we obtain $\lambda_{ph} = 0.46$, which implies weak coupling SC in Nb_5Sn_2Al . This is consistent with the low value of $\Delta C_{el}/\gamma T_c$.

3.5. Critical fields and superconducting parameters

Figure 5(a) shows the isothermal magnetization curves at various temperatures for Nb_5Sn_2Al . The effective lower critical field B_{c1}^* at each temperature is defined as the value at which the curve deviates from its initial linear behavior. The resulting B_{c1}^* is plotted as a function of temperature in Fig. 5(b), and the extrapolation of the data to zero temperature yields $B_{c1}^*(0) = 1.4$ mT [26]. After correction for the demagnetization factor, we obtain the zero-temperature lower critical field $B_{c1}(0) = B_{c1}^*(0)/(1 - N_d) = 2.0$ mT. Figure 5(c) shows the temperature dependence of resistivity for Nb_5Sn_2Al under various magnetic fields. With increasing field, the resistive transition is gradually suppressed to lower temperatures, as expected. Following the same criterion as shown above (see Subsection 3.2.), we determine T_c for each field as the temperature at which zero resistivity is achieved, and plot the data in Fig. 5(d). Extrapolation of the upper critical field B_{c2} to zero temperature, using the Wathamer-Helfand-Hohenberg (WHH) theory [27], gives $B_{c2}(0) = 0.3$ T.

With $B_{c1}(0)$ and $B_{c2}(0)$ determined, we can estimate various superconducting parameters of Nb_5Sn_2Al . The Ginzburg-Landau (GL) coherence length $\xi_{GL}(0)$ as $\xi_{GL}(0) = \sqrt{\Phi_0/2\pi B_{c2}(0)} = 32.8$ nm, where $\Phi_0 = 2.07 \times 10^{-15}$ Wb is the flux quantum. Then from the equations $B_{c1}(0)/B_{c2}(0) = (\ln\kappa_{GL} + 0.5)/(2\kappa_{GL}^2)$ [28] and $B_{c1}(0) = (\Phi_0/4\pi\lambda_{eff}^2)(\ln\kappa_{GL} + 0.5)$, $\kappa_{GL} = 15.6$ and $\lambda_{eff} = 516$ nm are obtained.

4. Discussion

Now let us compare the physical properties of isostructural Nb_5Sn_2Al and Ti_5Sn_2Al , which are summarized in Table 2. As noted above, the γ value of Ti_5Sn_2Al is $\sim 60\%$ larger than that of Nb_5Sn_2Al . This means that Ti_5Sn_2Al has a considerably higher $N(E_F)$, yet no SC is observed. To gain more insight, we plot the T_c against the average number of valence electrons per atom ratio (e/a) for all known " W_5Si_3 "-type superconductors. According to the empirical rule proposed by Matthias [29], T_c of intermetallic superconductors is expected to exhibit two maxima at e/a close to 5 and 7 [29]. Indeed, as can be seen from the figure, most of the " W_5Si_3 "-type superconductors have e/a in the range between 4.25 and 4.625, although T_c is generally higher for superconductors containing group IVB elements than those containing group VB elements. Furthermore, in the latter case, a T_c maximum is found at $e/a \sim 4.5$, which is slightly lower than the empirical value of 4.7 [29]. These results suggest that this family of superconductors follows the Matthias rule and their T_c is mainly controlled by the band filling rather than $N(E_F)$. In this respect, the absence of SC in Ti_5Sn_2Al can be explained since its e/a of 3.875 appears to fall below the lower bound for SC. On the other hand, the e/a of W_5Si_3 exceeds the above range and reaches 5.25, hinting at the existence of another T_c maximum at higher valence electron account.

Finally, we note that, despite similar Nb atom chains, the T_c of Nb_5Sn_2Al is nearly one order of magnitude smaller than that of Nb_3Sn . This corroborates the previous notion that the presence of these one-dimensional chains is not a sufficient condition for achieving high T_c [4, 5]. Instead, it is pointed out that the λ_{ph} value of Nb_5Sn_2Al is only about one-third that of Nb_3Sn [30], which highlights the importance of electron phonon interaction in enhancing T_c .

5. Conclusion

In summary, we have studied the transport, magnetic and thermodynamic properties of isostructural Nb_5Sn_2Al and Ti_5Sn_2Al . The results demonstrate that Nb_5Sn_2Al is a type-II superconductor with a bulk T_c of 2.0 K and a non-BCS gap, while Ti_5Sn_2Al remains metallic down to 0.5 K. Surprisingly, compared with Nb_5Sn_2Al , Ti_5Sn_2Al has a even larger Sommerfeld coefficient, suggesting that the absence of SC is not due to a reduction in $N(E_F)$. Nevertheless, these results are in line with the empirical rule based on the average number of valence electrons per atom, and at the value of ~ 4.5 a T_c maximum is found for the " W_5Si_3 "-type superconductors. Further studies to increase the number of valence electrons and electron phonon coupling, which may result in higher T_c , are highly desirable in future.

Acknowledgments

This work is supported by the National Key Research and Development Program of China (No.2017YFA0303002) and the Fundamental Research Funds for the Central Universities of China.

References

- [1] Matthias B T, Geballe T H, and Compton V B 1963 *Rev. Mod. Phys.* **35**, 1.
- [2] Dew-Hughes D 1975 *Cryogenics* **15**, 435.
- [3] Havinga E E, Van Maaren M H, and Damsma H 1969 *Phys. Lett. A* **29**, 109.
- [4] Claeson T, Ivarsson J, and Rasmussen S E 1977 *J. Appl. Phys.* **48**, 3998.
- [5] Willis J O and Waterstrat R M 1979 *J. Appl. Phys.* **50**, 2863.
- [6] Pesliev P, Gyurov G, and Soyanchev R 1986 *Izv. Khim.* **19**, 267.
- [7] Shishido T, Ukei K, Toyota N, Sasaki T, Watanabe Y, Motai K, Fukuda T, Takeya H, and Takei H 1989 *J. Cryst. Growth* **96**, 1.
- [8] Shishido T, Ye J H, Toyota N, Ukei K, Sasaki T, Horiuchi H, and Fukuda T 1989 *Jpn. J. Appl. Phys.* **28**, 1519.
- [9] Kawashima K, Muranaka T, Kousaka Y, Akutagawa S, and Akimitsu J 2009 *J. Phys.: Conf. Ser.* **150**, 052106.
- [10] Machado A J S, Costa A M S, Nunes C A, dos Santos C A M, Grant T, and Fisk Z 2011 *Solid State Commun.* **151**, 1455.
- [11] Fukuma M, Kawashima K, Maruyama M, and Akimitsu J 2011 *J. Phys. Soc. Jpn.* **80**, 024702.
- [12] Lv B, Zhu X Y, Lorenz B, Wei F Y, Xue Y Y, Yin Z P, Kotliar G, and Chu C W 2013 *Phys. Rev. B* **88**, 134520.
- [13] Xie W W, Luo X H, Seibel E, Nielsen M, and Cava R 2015 *Chem. Mater.* **27**, 4511.
- [14] Xie W W, Luo X H, Phelan B F, and Cava R J 2015 *J. Mater. Chem. C* **3**, 8235.
- [15] McGuire M A and Parker D S 2016 *Phys. Rev. B* **93**, 064507.
- [16] Li S, Liu X Y, Anand V, and Lv B 2018 *New J. Phys.* **20**, 013009.
- [17] Bottcher P, Doert Th., Druska Ch., and Bradtmoller S 1997 *J. Alloy Compd.* **246**, 209.
- [18] Aronsson B 1955 *Acta Chem. Scand.* **9**, 1107.
- [19] Garcia E and Corbett J D 1988 *J. Solid State Chem.* **73**, 440.
- [20] Paduani C 2009 *Solid State Commun.* **149**, 1269.
- [21] Pietzk M A and Schuster J C 1995 *J. Alloy Compd.* **230**, L10.
- [22] Bardeen J, Cooper L N, and Schreiffer J R 1957 *Phys. Rev.* **108**, 1175.
- [23] Bouquet F, Fisher R A, Phillips N E, Hinks D G, and Jorgensen J D 2001 *Phys. Rev. Lett.* **87**, 047001.
- [24] Nakajima Y, Nakagawa T, Tamegai T, and Harima H 2008 *Phys. Rev. Lett.* **100**, 157001.
- [25] McMillan W L 1968 *Phys. Rev.* **167**, 331.
- [26] M. Tinkham 1975 *Introduction to superconductivity* (McGraw-Hill, New York).
- [27] Werthamer N R, Helfand E, and Hohenberg P C 1966 *Phys. Rev.* **147**, 295.
- [28] Hu C R 1972 *Phys. Rev. B* **6**, 1756.
- [29] Matthias B T 1955 *Phys. Rev.* **97**, 74.
- [30] Tutuncu H M, Srivastava G P, Bagci S, and Duman S 2006 *Phys. Rev. B* **74**, 212506.

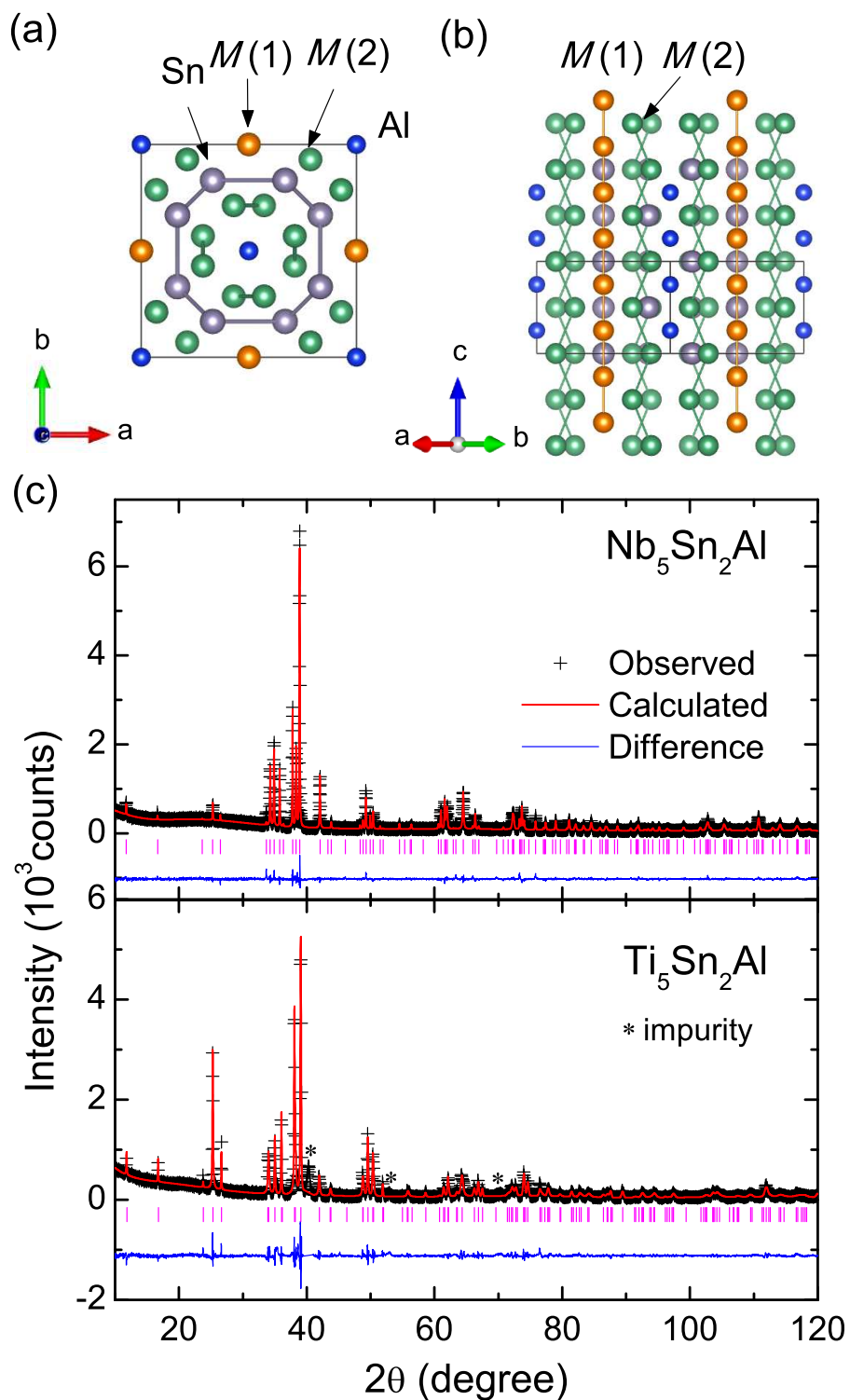


Figure 1. Schematic structure of M_5Sn_2Al projected perpendicular (a) and parallel (b) to the M atom chains. (c) Powder x-ray diffraction patterns and their refinement profiles at room temperature for Nb_5Sn_2Al and Ti_5Sn_2Al . The asterisks mark the impurity phases in the Ti_5Sn_2Al sample.

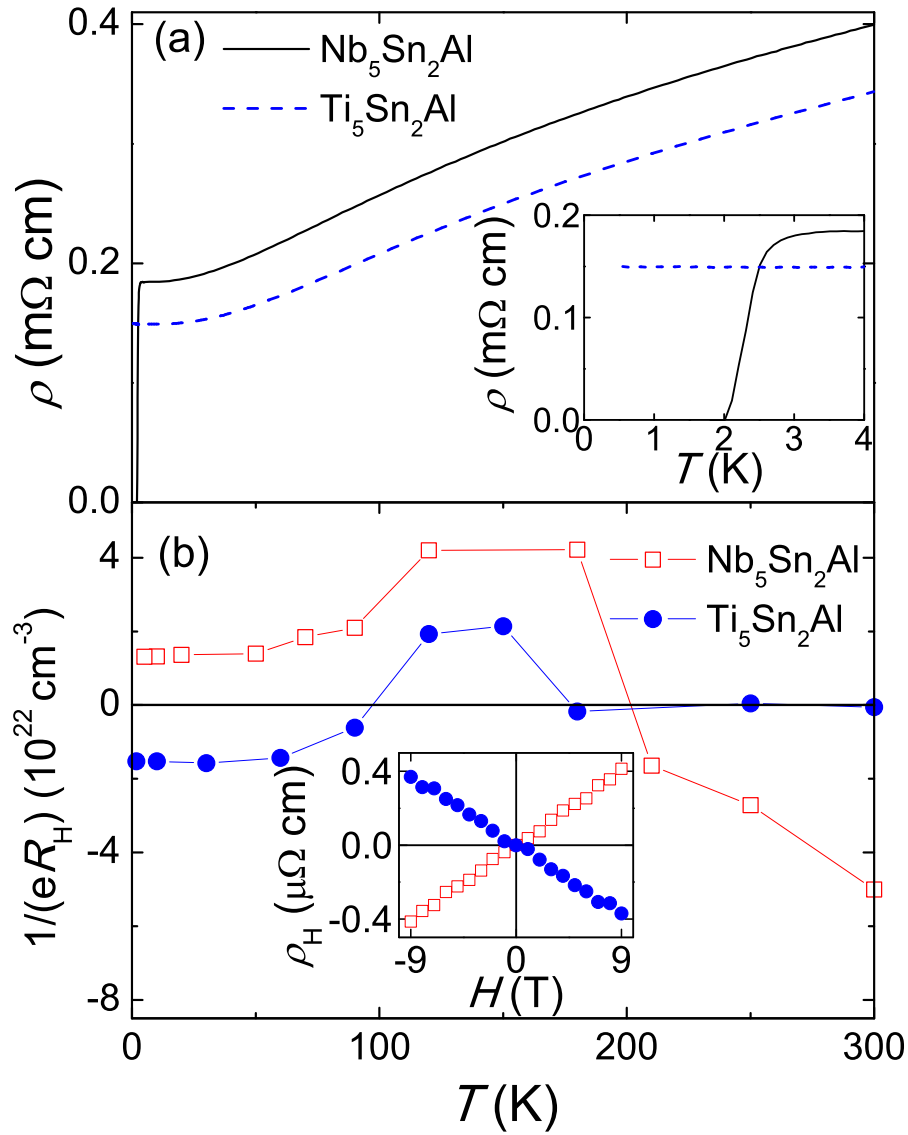


Figure 2. (a) Temperature dependence of resistivity for Nb_5Sn_2Al (solid line) and Ti_5Sn_2Al (dashed line). The inset shows a zoom of the low temperature data below 4 K. (b) Temperature dependence of inverse Hall coefficient for the two samples. The inset shows the field dependence of Hall resistivity for these samples at 10 K.

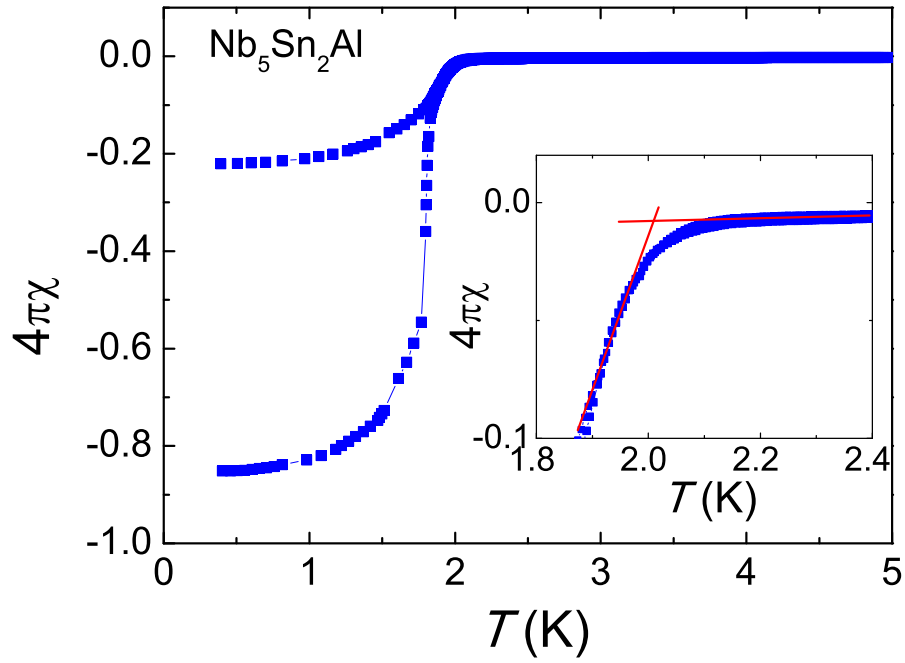


Figure 3. Temperature dependence of magnetic susceptibility below 5 K measured under an applied field of 0.45 mT. The inset shows a zoom of the data between 1.8 and 2.4 K. The two solid lines are a guide to the eyes.

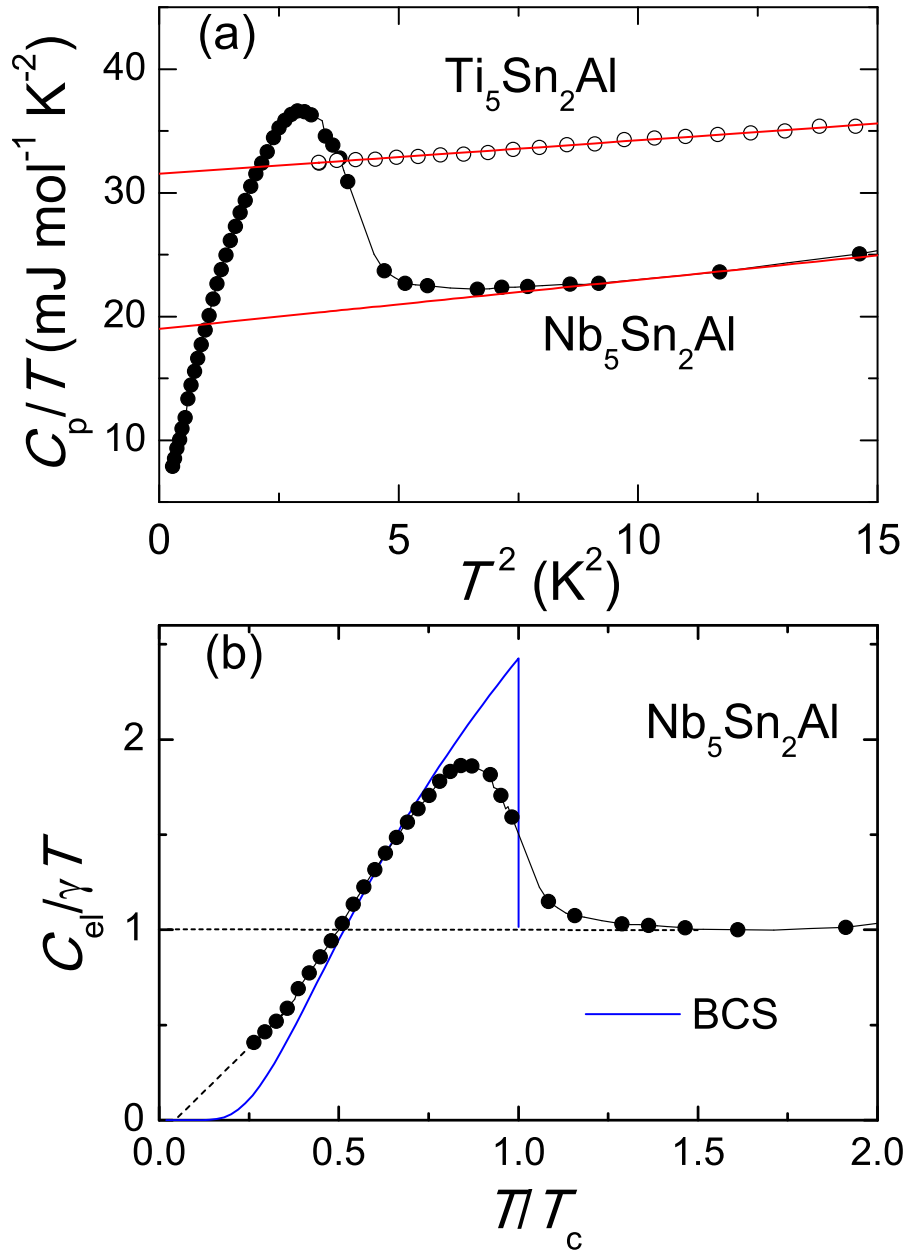


Figure 4. (a) Low temperature specific-heat data of Nb_5Sn_2Al and Ti_5Sn_2Al plotted as C_p/T versus T^2 . The solid lines are fits by the Debye model to the data (see text). (b) Normalized electronic specific heat for Nb_5Sn_2Al . The solid line denotes the theoretical BCS curve. The dashed lines are a guide to the eyes.

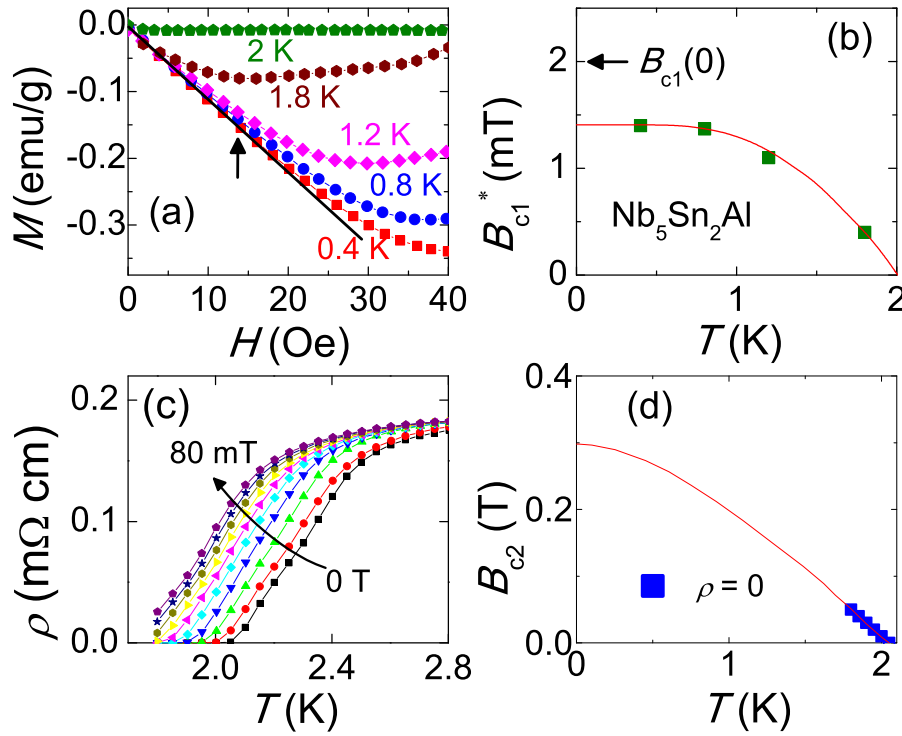


Figure 5. (a) Field dependence of magnetization curves for the Nb_5Sn_2Al sample measured after zero-field cooling to various temperatures. The solid line denotes the initial linear behavior and the arrow marks the deviation from this linearity at 0.4 K. (b) Temperature dependence of the effective lower critical field B_{c1}^* . The solid line is a fit to the data using the local dirty limit formula. The arrow marks the zero-temperature upper critical field $B_{c1}(0)$ after correction for the demagnetization factor. (c) Temperature dependence of resistivity for the Nb_5Sn_2Al sample under various magnetic fields up to 80 mT in increment of 10 mT. (d) The upper critical field B_{c2} plotted as a function of temperature for Nb_5Sn_2Al . The solid line is a WHH fit to the data.

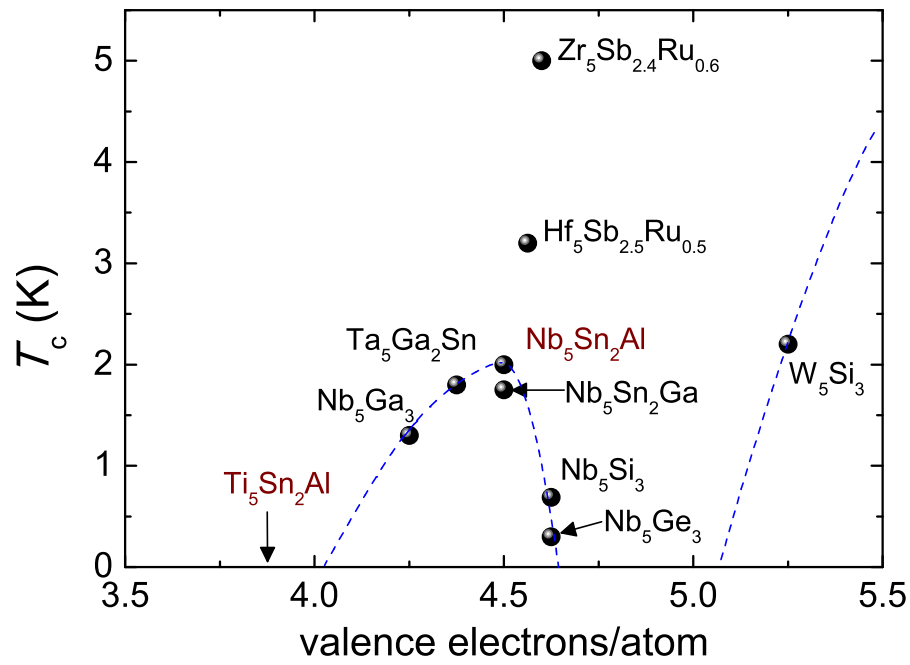


Figure 6. The superconducting transition temperature T_c plotted as a function of the average number of valence electrons per atom ratio for all known " W_5Si_3 "-type superconductors. The dashed lines are a guide to the eyes.

Table 1. Refined structural parameters of M_5Sn_2Al ($M = Nb, Ti$). Here a and c are the lattice parameters, V the unit cell volume, R_{wp} and R_p the weighted and unweighted R factors.

		Nb ₅ Sn ₂ Al	Ti ₅ Sn ₂ Al			
Space group		$I4/mcm$				
a (Å)		10.638(1)	10.558(2)			
c (Å)		5.225(1)	5.262(1)			
V (Å ³)		591.46	586.57			
R_{wp}		8.1%	12.9%			
R_p		5.7%	9.6%			
Atoms	site	x	y	z		
$M1$	16k	0.07308	0.2134	0		
$M2$	4b	0	0.5	0.25		
Sn	8h	0.1683	0.6683	0		
Al	4a	0	0	0.25		

Table 2. Physical parameters of Nb_5Sn_2Al and Ti_5Sn_2Al . Here T_c is the superconducting transition temperature, $B_{c1}(0)$ and $B_{c2}(0)$ the zero-temperature lower and upper critical fields for type-II superconductors, λ_{eff} the effective penetration depth, $\xi_{\text{GL}}(0)$ the Ginzburg-Landau coherence length, κ_{GL} the Ginzburg-Landau parameter, Θ_D the Debye temperature, γ the Sommerfeld coefficient, λ_{ph} the electron-phonon coupling constant.

Parameters	Nb_5Sn_2Al	Ti_5Sn_2Al
T_c (K)	2.0	—
$B_{c1}(0)$ (mT)	2.0	—
$B_{c2}(0)$ (T)	0.3	—
λ_{eff} (nm)	516	—
$\xi_{\text{GL}}(0)$ (nm)	32.8	—
κ_{GL}	15.6	—
Θ_D (K)	340	386
γ (mJ mol $^{-1}$ K $^{-2}$)	19.0	31.5
λ_{ph}	0.46	—